Nomenclature

A	amplitude of Tollmien-Schlichting wave
$a_{m,k}$	Landau coefficient governing growth of Tollmien-Schlichting wave
B	amplitude of Dean vortex
$b_{m,k}$	Landau coefficient governing growth of Dean vortex
f	nondimensional steady-state streamwise-velocity distribution
$g_{m,k}$	Landau coefficient governing phase of Tollmien-Schlichting wave
h	channel half-width
$h_{m,k}$	Landau coefficient governing phase of Dean vortex
i	imaginary part of complex number, $\sqrt{-1}$
$\mathbf{L}_{n,l}$	linear operator
$\mathbf{M}$	"mass" matrix
P	sum of base and perturbation pressure
p	perturbation pressure
$\mathbf{q}$	perturbation velocity-pressure vector
R	Reynolds number, $\overline{U}^* h^*/\nu^*$
$\mathbf{R}_s$	right-hand-side vector
r	radial (wall normal) coordinate
t	time
U	sum of base and perturbation velocity
$\mathbf{U}$	vector sum of base and perturbation velocity
$\overline{U}^*$	bulk velocity–volumetric flow rate divided by cross-sectional area
u	perturbation velocity
z	axial (spanwise) coordinate
$\aleph$	azimuthal wave number
β	axial wave number
γ	phase of Tollmien-Schlichting wave
ζ	phase of Dean vortex
η	curvature parameter (ratio of inner to outer radii)
θ	azimuthal (streamwise) coordinate
κ_s	complex Landau coefficient from equation system s
λ	curvature parameter, $1 - \eta$
ν	kinematic viscosity
ρ	density
χ^0	portion of nonlinear correction proportional to linear solution
χ^1	portion of nonlinear correction linearly independent of linear solution

$\overline{\omega}_r$	radial component of χ^1
∇	gradient operator

Subscripts:

c	center
i	inner
k	nonlinear correction due to vortex
l	multiple of spanwise wave number of vortex
m	nonlinear correction due to streamwise wave
n	multiple of streamwise wave number
o	outer
r	radial (wall normal)
s	equation system number
z	axial (spanwise)
θ	azimuthal (streamwise)

Superscripts:

k	nonlinear correction due to vortex
l	multiple of spanwise wave number of vortex
m	nonlinear correction due to streamwise wave
n	multiple of streamwise wave number
$*$	dimensional quantity

Abbreviations:

DHZ	Daudpota, Hall, and Zang (see ref. 10)
DNS	direct numerical simulation
TS	Tollmien-Schlichting

Abstract

A weakly nonlinear theory is developed to study the interaction of Tollmien-Schlichting (TS) waves and Dean vortices in curved channel flow. The predictions obtained from the theory agree well with results obtained from direct numerical simulations of curved channel flow, especially for low-amplitude disturbances. Some discrepancies in the results of a previous theory with direct numerical simulations are resolved.

1. Introduction

Interactions between Tollmien-Schlichting (TS) waves and streamwise vortices can be an important part of the transition process (ref. 1). Kim and Moser (ref. 2) and Singer, Reed, and Ferziger (ref. 3) showed that weak streamwise vortices can alter the mode by which the flow undergoes transition. Nayfeh and Al-Maaitah (ref. 4) used Floquet theory to study the influence of Görtler vortices on the growth of oblique TS waves. They found that there are two components to the solution; one is stabilized and the other is destabilized by the presence of the vortices. Malik and Hussaini (ref. 5) studied the interactions of Görtler vortices and TS waves via direct numerical simulations. They found qualitative agreement with the results of Nayfeh and Al-Maaitah (ref. 4).

A series of studies on the interactions of TS waves and streamwise vortices in curved channel flows at asymptotically high Reynolds number have been made (refs. 6–9). Daudpota, Hall, and Zang (ref. 10) (hereinafter referred to as DHZ) developed a weakly nonlinear interaction theory to study the interaction at a finite Reynolds number. They employed a multiple-scale version of the approach developed by Stuart (ref. 11) and Watson (ref. 12) to derive two coupled Landau equations for the perturbation amplitudes of the streamwise vortices (called Dean vortices in curved channel flow) and TS waves. A comparison of their theoretical predictions with the results of direct numerical simulation (ref. 13) suggests that their results are in error with respect to the influence of the TS wave on the Dean vortex. The resolution of this discrepancy is a major motivation for undertaking this work.

In section 2 we present a slightly different formulation (see refs. 14 and 15 by Herbert) of a weakly nonlinear interaction theory and describe how the resulting equations are solved. We also include suggestions to guide the intelligent use of the theory. In section 3 we compare the results from the current theory with results from DHZ. In addition, direct numerical simulation is used to verify that the current theory correctly predicts the overall behavior of the flow. Finally, in section 4 we draw conclusions.

The authors would like to thank Thorwald Herbert of Ohio State University, Q. Isa Daudpota, formerly NRC at the Langley Research Center, and Philip Hall of the University of Manchester, UK, for many useful discussions.

2. Mathematical Formulation

2.1. The Basic Equations

The incompressible Navier-Stokes equations in cylindrical coordinates (r^*, θ, z^*) are written as

$$\frac{1}{r^*}\frac{\partial\left(r^* U_r^*\right)}{\partial r^*} + \frac{1}{r^*}\frac{\partial U_\theta^*}{\partial \theta} + \frac{\partial U_z^*}{\partial z^*} = 0 \tag{1}$$

$$\frac{\partial U_r^*}{\partial t^*} + \left(\mathbf{U}^* \cdot \nabla^*\right) U_r^* - \frac{1}{r^*} U_\theta^{*2} = -\frac{1}{\rho^*}\frac{\partial P^*}{\partial r^*} + \nu^* \left(\nabla^{*2} U_r^* - \frac{U_r^*}{r^{*2}} - \frac{2}{r^{*2}}\frac{\partial U_\theta^*}{\partial \theta}\right) \tag{2}$$

$$\frac{\partial U_\theta^*}{\partial t^*} + \left(\mathbf{U}^* \cdot \nabla^*\right) U_\theta^* + \frac{U_\theta^* U_r^*}{r^*} = -\frac{1}{r^* \rho^*}\frac{\partial P^*}{\partial \theta} + \nu^* \left(\nabla^{*2} U_\theta^* - \frac{U_\theta^*}{r^{*2}} + \frac{2}{r^{*2}}\frac{\partial U_r^*}{\partial \theta}\right) \tag{3}$$

$$\frac{\partial U_z^*}{\partial t^*} + (\mathbf{U}^* \cdot \nabla^*) U_z^* = -\frac{1}{\rho^*}\frac{\partial P^*}{\partial z^*} + \nu^* \nabla^{*2} U_z^* \tag{4}$$

where

$$\mathbf{U}^* \cdot \nabla^* = U_r^* \frac{\partial}{\partial r^*} + \frac{U_\theta^*}{r^*}\frac{\partial}{\partial \theta} + U_z^* \frac{\partial}{\partial z^*} \tag{5}$$

$$\nabla^{*2} = \frac{1}{r^*}\frac{\partial}{\partial r^*}\left(r^* \frac{\partial}{\partial r^*}\right) + \frac{1}{r^{*2}}\frac{\partial^2}{\partial \theta^2} + \frac{\partial^2}{\partial z^{*2}} \tag{6}$$

and ρ^* and ν^* represent the constant density and kinematic viscosity, respectively. The asterisks indicate dimensional quantities. The geometry of the problem of azimuthal flow between infinite concentric walls of outer radius r_o^* and inner radius r_i^* is illustrated in figure 1. The wall boundary conditions require that

$$U_r^* = U_\theta^* = U_z^* = 0 \qquad (r^* = r_i^*, r_o^*) \tag{7}$$

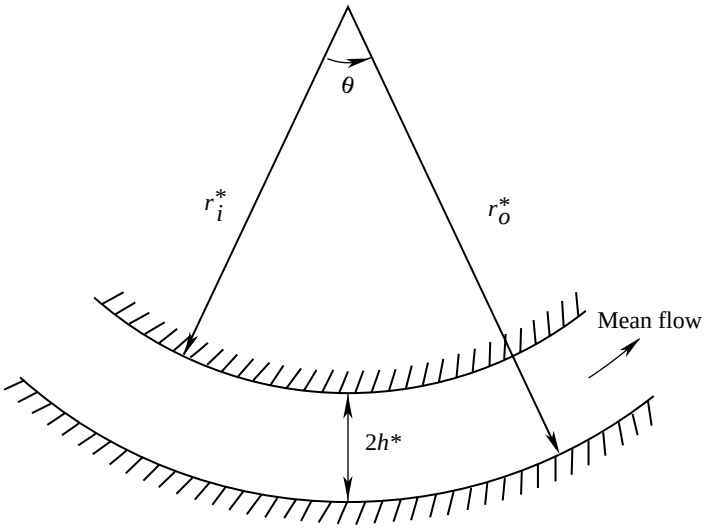

Figure 1. Curved channel flow geometry.

A solution to the equations gives $(U_r^*, U_\theta^*, U_z^*, P^*)$ as

$$\begin{pmatrix} U_r^* \\ U_\theta^* \\ U_z^* \\ P^* \end{pmatrix} = \begin{pmatrix} 0 \\ \overline{U}^* f(r^*) \\ 0 \\ 2\theta\nu\rho D^* \overline{U}^* + \rho^* \overline{U}^{*2} \int \frac{f(r^*)^2}{r^*} dr^* \end{pmatrix} \tag{8}$$

Here, $\overline{U}^*$ is the bulk velocity and

$$f(r^*) = D^* \left[r^* \log\left(\frac{r^*}{h^*}\right) + C^* r^* + \frac{E^*}{r^*} \right]$$

where

$$D^* = -\frac{2}{r_c^* + \frac{E^*}{h^*}\log\eta} \tag{9}$$

$$C^* = \frac{r_i^{*2}\log\left(\frac{r_i^*}{h^*}\right) - r_o^{*2}\log\left(\frac{r_o^*}{h^*}\right)}{r_o^{*2} - r_i^{*2}} \tag{10}$$

$$E^* = -\frac{(r_i^* r_o^*)^2}{r_o^{*2} - r_i^{*2}}\log\eta \tag{11}$$

The quantity $r_c^* = (r_o^* + r_i^*)/2$ is the centerline radius, $h^* = (r_o^* - r_i^*)/2$ is the channel half-width, and the ratio $\eta = r_i^*/r_o^*$ describes the channel curvature.

We nondimensionalize all spatial coordinates with the channel half-width, velocities with the bulk velocity, and pressure with $\rho^*\overline{U}^{*2}$. The temporal scale is $h^*/\overline{U}^*$. The Reynolds number is defined as

$$R = \frac{\overline{U}^* h^*}{\nu^*}$$

The nondimensional equations are easily obtained from the dimensional ones by replacing all starred quantities with their corresponding nondimensional unstarred ones and noting that $\rho = 1$, $h = 1$, and $\nu = 1/R$. The expression $1-\eta$ appears often below and is denoted by λ. When $\lambda = \lambda_c = 2.179\times10^{-5}$, the minimum Reynolds number for instability of TS waves is the same as that for Dean vortices (ref. 16).

We follow closely the perturbation method introduced by Herbert (refs. 14 and 15), extending it to the case of interacting disturbances. The steady solution is perturbed such that

$$\begin{pmatrix} U_r \\ U_\theta \\ U_z \\ P \end{pmatrix} = \begin{pmatrix} 0 \\ f(r) \\ 0 \\ 2D\theta + \int \frac{f^2}{r}dr \end{pmatrix} + \begin{pmatrix} u_r \\ u_\theta \\ u_z \\ p \end{pmatrix} \tag{12}$$

where u_r, u_θ, u_z, and p are disturbance quantities. Where appropriate, the disturbance vector will be written as

$$\mathbf{q} = \begin{pmatrix} u_r \\ u_\theta \\ u_z \\ p \end{pmatrix} \tag{13}$$

Substituting the perturbations into the nondimensionalized Navier-Stokes equations, subtracting the steady-flow component, and rearranging gives

$$\frac{1}{r}\frac{\partial(ru_r)}{\partial r} + \frac{1}{r}\frac{\partial u_\theta}{\partial\theta} + \frac{\partial u_z}{\partial z} = 0 \tag{14}$$

$$\frac{\partial u_r}{\partial t} + \frac{\partial p}{\partial r} - \frac{2f}{r}u_\theta + \frac{f}{r}\frac{\partial u_r}{\partial\theta} - \frac{1}{R}\left(\nabla^2 u_r - \frac{u_r}{r^2} - \frac{2}{r^2}\frac{\partial u_\theta}{\partial\theta}\right) = -(\mathbf{U}\cdot\nabla)u_r + \frac{1}{r}u_\theta^2 \tag{15}$$

$$\frac{\partial u_\theta}{\partial t} + \frac{1}{r}\frac{\partial p}{\partial\theta} + \frac{fu_r}{r} + \frac{f}{r}\frac{\partial}{\partial\theta}u_\theta + (\mathbf{U}\cdot\nabla)f - \frac{1}{R}\left(\nabla^2 u_\theta - \frac{u_\theta}{r^2} + \frac{2}{r^2}\frac{\partial u_r}{\partial\theta}\right) = -(\mathbf{U}\cdot\nabla)u_\theta - \frac{u_\theta u_r}{r} \tag{16}$$

$$\frac{\partial u_z}{\partial t} + \frac{\partial p}{\partial z} + \frac{f}{r}\frac{\partial u_z}{\partial\theta} - \frac{1}{R}\nabla^2 u_z = -(\mathbf{U}\cdot\nabla)u_z \tag{17}$$

where

$$\mathbf{U}\cdot\nabla = u_r\frac{\partial}{\partial r} + \frac{u_\theta}{r}\frac{\partial}{\partial\theta} + u_z\frac{\partial}{\partial z} \tag{18}$$

$$\nabla^2 = \frac{1}{r}\frac{\partial}{\partial r}\left(r\frac{\partial}{\partial r}\right) + \frac{1}{r^2}\frac{\partial^2}{\partial \theta^2} + \frac{\partial^2}{\partial z^2} \tag{19}$$

We are considering here the idealized problem in which the solution is periodic in the azimuthal (streamwise) and axial (spanwise) directions and the solution evolves in time. In addition, the mean pressure gradient is kept constant.

2.2. Fourier Expansions

The linearized disturbance equations are obtained by setting the right-hand sides of equations (14)–(17) equal to zero. A solution to the equations for a two-dimensional (2D) TS wave can be written as

$$\mathbf{q} = \tilde{\mathbf{q}}_{1,0}(r,t)\; e^{i[\aleph\theta - \gamma(t)]} \tag{20}$$

Here $\aleph$ is real and represents the azimuthal wave number, whereas $\gamma(t)$ is a real function defining the phase. Any growth or decay of the linearized TS wave is expressed in terms of the amplitude such that

$$\tilde{\mathbf{q}}_{1,0}(r,t) = A(t)\; \hat{\mathbf{q}}_{1,0,0,0}(r) \tag{21}$$

where

$$\frac{dA}{dt} = a_{0,0}A \tag{22}$$

and $a_{0,0}$ is the linear growth rate. Quantities of the form $\hat{\mathbf{q}}_{n,m,l,k}$ are used frequently throughout the report. The n and l indices refer to multiples of the TS and/or Dean wave numbers, whereas the m and k indices refer to the order of the nonlinear corrections. For instance, $\hat{\mathbf{q}}_{1,0,0,0}$ is the zeroth-order correction of the primary TS wave number, in other words, the TS linear eigenfunction. We define the amplitude as

$$A(t) = \frac{|\tilde{u}_r^{1,0}(r_c,t)|}{|\hat{u}_r^{1,0,0,0}(r_c)|} \tag{23}$$

where r_c is the channel centerline. In general, the amplitude represents the ratio of the magnitude of any perturbation quantity and the magnitude of the corresponding linear eigenfunction quantity. The amplitude definition can be varied independently of the normalization of the linear eigenfunction. This is somewhat more general than that done by Herbert (refs. 14 and 15). The importance of this generalization will be made clear later when we discuss alternative definitions of the amplitude. Here, we normalize the linear eigenfunction by taking

$$\hat{u}_r^{1,0,0,0}(r_c) = 1 \tag{24}$$

In a similar manner, one can write the solution for the primary Dean vortex mode as

$$\mathbf{q} = \tilde{\mathbf{q}}_{0,1}(r,t)\; e^{i[\beta z - \zeta(t)]} \tag{25}$$

where β is the real axial wave number and $\zeta(t) = 0$ indicates that the linear Dean disturbance is stationary. We also write

$$\tilde{\mathbf{q}}_{0,1}(r,t) = B(t)\; \hat{\mathbf{q}}_{0,0,1,0}(r) \tag{26}$$

where

$$\frac{dB}{dt} = b_{0,0}B \tag{27}$$

The amplitude is defined such that

$$B(t) = \frac{|\tilde{u}_r^{0,1}(r_c,t)|}{|\hat{u}_r^{0,0,1,0}(r_c)|} \tag{28}$$

and the eigenfunction is normalized so that

$$\hat{u}_r^{0,0,1,0}(r_c) = 1 \tag{29}$$

When the nonlinear terms (the right-hand sides of eqs. (14)–(17)) are included, the disturbances can interact with themselves, with the mean flow, with each other, and with all the relevant complex conjugates. This results in the generation of harmonics, mean-flow distortions, and various corrections to the fundamental disturbances. Hence, it is natural to expand the perturbation variables in the double Fourier series:

$$\mathbf{q} = \sum_{n=-\infty}^{\infty} \sum_{l=-\infty}^{\infty} \tilde{\mathbf{q}}_{n,l}(r,t)\ e^{in[\aleph\theta - \gamma(t)]} e^{il[\beta z - \zeta(t)]} \tag{30}$$

2.3. Amplitude Expansion

The nonlinear partial differential equations obtained by substituting equation (30) into equations (14)–(17) are coupled and difficult to solve efficiently. We seek a solution by expanding $\tilde{\mathbf{q}}_{n,l}$ in the amplitude parameters $A(t)$ and $B(t)$ about the linear solutions given by equations (20) and (25). The solutions will reflect the deviations from linear behavior for finite, but sufficiently small, amplitudes A and B. In this context, all harmonics of the primary disturbances are considered to be forced. Since the linear TS and Dean solutions are $O(A)$ and $O(B)$, respectively, their first harmonics and cross terms will be $O(A^2)$, $O(B^2)$, and $O(AB)$. Higher order harmonics and cross terms will be $O(A^n B^l)$; hence, it is reasonable to let

$$\tilde{\mathbf{q}}_{n,l}(r,t) = A^{|n|} B^{|l|}\ \tilde{\tilde{\mathbf{q}}}_{n,l}(r,t) \tag{31}$$

where all double tilde terms are $O(1)$ except for those with $n = l = 0$. Heuristically, one can see that the exception with the $n = l = 0$ term comes about from the fact that the lowest order mean-flow distortions are generated from the product of either TS or Dean fundamental disturbances with their respective complex conjugates. The fundamental disturbances are $O(A)$ and $O(B)$; hence, the product terms that generate $n = l = 0$ are $O(A^2)$ and $O(B^2)$, respectively.

Substitution of the representation in equation (31) into equation (30) yields

$$\mathbf{q} = \sum_{n=-\infty}^{\infty} \sum_{l=-\infty}^{\infty} \tilde{\tilde{\mathbf{q}}}_{n,l}(r,t)\ A^{|n|}(t)\ B^{|l|}(t)\ e^{in[\aleph\theta - \gamma(t)]} e^{il[\beta z - \zeta(t)]} \tag{32}$$

We now expand the double tilde representations into sums that are products of ascending powers of the amplitude functions with coefficients which are strictly functions of the radial coordinate. In the limit, as $A \to 0$ and $B \to 0$, the solutions tend toward the linear results. Only even powers of A and B are needed (Drazin and Reid in ref. 17) because of the invariance of the original equations and boundary conditions with respect to arbitrary translation in the streamwise and spanwise directions and the assumption of periodicity of the solutions in these directions. Hence,

$$\tilde{\tilde{\mathbf{q}}}_{n,l}(r,t) = \sum_{m=0}^{\infty} \sum_{k=0}^{\infty} \hat{\mathbf{q}}_{n,m,l,k}(r)\ A^{2m}(t)\ B^{2k}(t) \tag{33}$$

By substitution into equation (32) one obtains the full representation of the perturbation vector:

$$\mathbf{q} = \sum_{n=-\infty}^{\infty} \sum_{m=0}^{\infty} \sum_{l=-\infty}^{\infty} \sum_{k=0}^{\infty} \hat{\mathbf{q}}_{n,m,l,k} A^{2m+|n|} B^{2k+|l|} e^{in(\aleph\theta - \gamma)} e^{il(\beta z - \zeta)} \tag{34}$$

In order that the wall boundary conditions be satisfied at all orders of approximation, we require that

$$\begin{pmatrix} \hat{u}_r^{n,m,l,k}(r) \\ \hat{u}_\theta^{n,m,l,k}(r) \\ \hat{u}_z^{n,m,l,k}(r) \end{pmatrix} = \begin{pmatrix} 0 \\ 0 \\ 0 \end{pmatrix} \tag{35}$$

at $r = r_i,\ r_o$ for all combinations of n, m, l, and k. The case $n = m = l = k = 0$ represents the basic flow which has already been considered so that $\hat{\mathbf{q}}_{0,0,0,0} = \mathbf{0}$.

Consistent expansions of the time derivatives $\dot{A}/A$, $\dot{B}/B$, $\dot{\gamma}$, and $\dot{\zeta}$ are in powers of A^2 and B^2 so that

$$\frac{\dot{A}}{A} = \sum_{m=0}^{\infty}\sum_{k=0}^{\infty} a_{m,k} A^{2m} B^{2k} \tag{36}$$

$$\frac{\dot{B}}{B} = \sum_{m=0}^{\infty}\sum_{k=0}^{\infty} b_{m,k} A^{2m} B^{2k} \tag{37}$$

$$\dot{\gamma} = \sum_{m=0}^{\infty}\sum_{k=0}^{\infty} g_{m,k} A^{2m} B^{2k} \tag{38}$$

$$\dot{\zeta} = \sum_{m=0}^{\infty}\sum_{k=0}^{\infty} h_{m,k} A^{2m} B^{2k} \tag{39}$$

Equations (36) and (37) are the coupled Landau equations that describe the growth of the disturbances. The purpose of the remainder of this section is to determine the Landau coefficients $a_{m,k}$ and $b_{m,k}$.

2.4. Solution Method

The solution expansions in equations (32)–(39) are substituted into the perturbation equations (14)–(17). All terms with common exponential factors are grouped together. The simplest nonlinear theory is obtained by considering only those terms with Fourier exponents limited by

$$-1 \le n \text{ and } l \le 2$$

With this restriction, it is only appropriate to consider terms in the amplitude expansions (eq. (33)) with $m = 0, 1$ and $k = 0, 1$. Larger values of m or k give higher order contributions that should not be considered at this degree of truncation. In each group with common exponential factors, all terms with common powers of A and B are collected. MACSYMA (ref. 18) was used to substantially reduce the chance of error in obtaining the final equations. Twelve systems of equations, indexed by s, remain to be solved numerically. A description of each of the systems is summarized in table 1.

Table 1. Summary of Equation Systems

Equation system number (s)	Order	n	m	l	k	Description
1	A	1	0	0	0	Linear TS wave
2	B	0	0	1	0	Linear Dean vortex
3	A^2	0	1	0	0	Mean-flow distortion from TS
4	B^2	0	0	0	1	Mean-flow distortion from Dean
5	A^2	2	0	0	0	TS harmonic
6	B^2	0	0	2	0	Dean harmonic
7	AB	1	0	1	0	TS—Dean cross harmonic
8	AB	1	0	-1	0	TS—Dean cross harmonic
9	A^3	1	1	0	0	Self-correction to TS
10	B^3	0	0	1	1	Self-correction to Dean
11	AB^2	1	0	0	1	Dean correction to TS
12	A^2B	0	1	1	0	TS correction to Dean

The first two equation systems ($s = 1$ and 2) are eigenvalue problems of the form

$$\mathbf{L}_{n,l}\hat{\mathbf{q}}_{n,0,l,0} = \left[n\left(a_{0,0} - ig_{0,0}\right) + l\left(b_{0,0} - ih_{0,0}\right)\right]\mathbf{M}\hat{\mathbf{q}}_{n,0,l,0} \tag{40}$$

where

$$\mathbf{M} = \begin{pmatrix} -1 & 0 & 0 & 0 \\ 0 & -1 & 0 & 0 \\ 0 & 0 & -1 & 0 \\ 0 & 0 & 0 & 0 \end{pmatrix} \tag{41}$$

The elements of the operator $\mathbf{L}_{n,l}$ are given in appendix A. The solution of the eigenvalue problem determines the most unstable eigenvalues, $a_{0,0} - ig_{0,0}$ and $b_{0,0} - ih_{0,0}$. The normalizations in equations (24) and (29) are used to uniquely define the eigenvectors $\hat{\mathbf{q}}_{1,0,0,0}(r)$ and $\hat{\mathbf{q}}_{0,0,1,0}(r)$. The eigenvalues are the zeroth-order Landau coefficients.

Equation systems 3 and 4 (i.e., $s = 3$ and 4) represent the mean-flow distortion caused by the TS and Dean disturbances, respectively. For this case, $n = l = 0$ and the operator $\mathbf{L}_{n,l}$ is greatly simplified. We consider the case where either m or k equals 1, while the other equals 0. The mean pressure gradient is constant; hence, $\hat{p}^{0,1,0,0} = \hat{p}^{0,0,0,1} = 0$. Analysis indicates that only the azimuthal velocity component of the mean-flow distortions is nonzero. Its equation is

$$\left(2ma_{0,0}+2kb_{0,0}+\frac{1}{r^2R}\right)\hat{u}_\theta^{0,m,0,k}-\frac{1}{rR}\frac{d}{dr}\hat{u}_\theta^{0,m,0,k}-\frac{1}{R}\frac{d^2}{dr^2}\hat{u}_\theta^{0,m,0,k}=ik\beta\left(\hat{u}_\theta^{0,0,-1,0}\hat{u}_z^{0,0,1,0}\right.$$
$$\left.-\hat{u}_\theta^{0,0,1,0}\hat{u}_z^{0,0,-1,0}\right)-\left(\hat{u}_r^{m,0,k,0}\hat{u}_\theta^{-m,0,-k,0}+\hat{u}_r^{-m,0,-k,0}\hat{u}_\theta^{m,0,k,0}\right)/r$$
$$-\left[\hat{u}_r^{m,0,k,0}\frac{d}{dr}\left(\hat{u}_\theta^{-m,0,-k,0}\right)+\hat{u}_r^{-m,0,-k,0}\frac{d}{dr}\left(\hat{u}_\theta^{m,0,k,0}\right)\right] \tag{42}$$

In similar contexts, Davey and Nguyen (ref. 19) and Herbert (ref. 15) point to an important restriction to the theory that results from equation (42). When either of the linear growth rates $a_{0,0}$ or $b_{0,0}$ are negative, the associated homogeneous problem with homogeneous boundary conditions can be recast as a Bessel equation through a change of variables. Hence, solutions of the homogeneous problem can exist and can contribute an arbitrarily large component to the solution of the forced problem. To prevent this difficulty we require both $a_{0,0}$ and $b_{0,0}$ to be nonnegative. This restricts the application of the theory to those regimes where both the TS and Dean disturbances are linearly unstable.

The equation systems 5–12 (i.e., $s = 5$–12) are all of the form

$$\left[\mathbf{L}_{n,l}-\left(2ma_{0,0}+|n|a_{0,0}-ing_{0,0}+2kb_{0,0}+|l|b_{0,0}-ilh_{0,0}\right)\mathbf{M}\right]\hat{\mathbf{q}}_{n,m,l,k}=\mathbf{R}_s \tag{43}$$

where $\mathbf{R}_s$ is the right-hand-side vector of the s equation system. The right-hand-side vectors consist of nonlinear combinations of the solutions obtained at lower order. The elements of the right-hand-side vectors $\mathbf{R}_s$ are given explicitly in appendix B.

Equation systems 5–8 (i.e., $s = 5$–8) for the various harmonics require numerically solving a sequence of linear, ordinary differential equation systems. In the case of Dean disturbances, we found that it is possible that the harmonic of an unstable mode is also in the unstable regime. When this happens, it violates the assumption that all the higher harmonics are forced by the primary disturbances. Although numerical results can be obtained for such cases, the results are meaningless since the harmonic can grow on its own and is not simply forced by the fundamental. We found that this circumstance does not occur for the TS waves.

Equation systems 9, 10, 11, and 12 (i.e., $s = 9$, 10, 11, and 12) define the corrections to the fundamental TS and Dean disturbances and allow us to calculate the Landau coefficients $a_{1,0}$, $b_{0,1}$, $a_{0,1}$, and $b_{1,0}$, respectively. It is in the solution of these terms that the method developed by Herbert (refs. 14 and 15) differs from the standard approach developed by Stuart (ref. 11) and Watson (ref. 12).

The right-hand-side vectors $\mathbf{R}_s$ for $s = 9$–12 can be rewritten as

$$\mathbf{R}_s=\mathbf{R}'_s+\kappa_s\mathbf{M}\hat{\mathbf{q}}_{n,0,l,0} \tag{44}$$

where

$$\kappa_9=a_{1,0}-ig_{1,0}$$
$$\kappa_{10}=b_{0,1}-ih_{0,1}$$
$$\kappa_{11}=a_{0,1}-ig_{0,1}$$
$$\kappa_{12}=b_{1,0}-ih_{1,0}$$

The correspondence between the index s and the indices n, m, l, and k is given in table 1. The solution vectors $\hat{\mathbf{q}}_{n,m,l,k}$ for these equation systems are the sums of particular solution vectors ; hence,

$$\hat{\mathbf{q}}_{n,m,l,k}(r)=\kappa_s\ \chi^0_{n,m,l,k}(r)+\chi^1_{n,m,l,k}(r) \tag{45}$$

where

$$\chi^0_{n,m,l,k}(r_i) = \chi^0_{n,m,l,k}(r_o) = \chi^1_{n,m,l,k}(r_i) = \chi^1_{n,m,l,k}(r_o) = 0 \tag{46}$$

Substitution of equations (44) and (45) into equation (43) leads to

$$\left\{\mathbf{L}_{n,l} - \left[2ma_{0,0} + n(a_{0,0} - ig_{0,0}) + 2kb_{0,0} + l(b_{0,0} - ih_{0,0})\right]\mathbf{M}\right\}\kappa_s\chi^0_{n,m,l,k} = \kappa_s\mathbf{M}\hat{\mathbf{q}}_{n,0,l,0} \tag{47}$$

and

$$\left\{\mathbf{L}_{n,l} - \left[2ma_{0,0} + n(a_{0,0} - ig_{0,0}) + 2kb_{0,0} + l(b_{0,0} - ih_{0,0})\right]\mathbf{M}\right\}\chi^1_{n,m,l,k} = \mathbf{R}'_s \tag{48}$$

Recognizing that

$$\left\{\mathbf{L}_{n,l} - \left[n(a_{0,0} - ig_{0,0}) + l(b_{0,0} - ih_{0,0})\right]\mathbf{M}\right\}\hat{\mathbf{q}}_{n,0,l,0} = 0 \tag{49}$$

when $(n = 1, l = 0)$ or $(n = 0, l = 1)$, one finds by inspection of equation (47) that

$$-\left(2ma_{0,0} + 2kb_{0,0}\right)\chi^0_{n,m,l,k} = \hat{\mathbf{q}}_{n,0,l,0} \tag{50}$$

or

$$\chi^0_{n,m,l,k} = -\frac{\hat{\mathbf{q}}_{n,0,l,0}}{2ma_{0,0} + 2kb_{0,0}} \tag{51}$$

It is straightforward to solve equation (48) numerically to obtain $\chi^1_{n,m,l,k}$. Substituting equation (51) into equation (45) gives

$$\hat{\mathbf{q}}_{n,m,l,k}(r) = \chi^1_{n,m,l,k}(r) - \frac{\kappa_s\ \hat{\mathbf{q}}_{n,0,l,0}(r)}{2ma_{0,0} + 2kb_{0,0}} \tag{52}$$

In order to determine the Landau coefficients κ_s, we use the amplitude definitions in equations (23) and (28). Together with the expansions in equations (31)–(34) they require that

$$\frac{|\tilde{u}^{1,0}_r(r_c,t)|}{|\hat{u}^{1,0,0,0}_r(r_c)|} = \frac{|\sum_{m=0}^{\infty}\sum_{k=0}^{\infty}A^{2m+1}B^{2k}\ \hat{u}^{1,m,0,k}_r(r_c)|}{|\hat{u}^{1,0,0,0}_r(r_c)|} = A(t) \tag{53}$$

and

$$\frac{|\tilde{u}^{0,1}_r(r_c,t)|}{|\hat{u}^{0,0,1,0}_r(r_c)|} = \frac{|\sum_{m=0}^{\infty}\sum_{k=0}^{\infty}A^{2m}B^{2k+1}\ \hat{u}^{0,m,1,k}_r(r_c)|}{|\hat{u}^{0,0,1,0}_r(r_c)|} = B(t) \tag{54}$$

For these to be correct at all orders of approximation,

$$\hat{u}^{1,m,0,k}_r(r_c) = 0 \tag{55}$$

for all $m, k > 0$ and

$$\hat{u}^{0,m,1,k}_r(r_c) = 0 \tag{56}$$

for all $m, k > 0$.

The conditions from equations (55) and (56) can now be used to determine κ_s. Let the radial velocity component of $\chi^1_{n,m,l,k}$ be $\overline{\omega}^{n,m,l,k}_r$. Equations (55) and (56) are applied in equation (52) to require

$$\overline{\omega}^{n,m,l,k}_r(r_c) - \frac{\kappa_s\ \hat{u}^{n,0,l,0}_r(r_c)}{2ma_{0,0} + 2kb_{0,0}} = 0 \tag{57}$$

Hence,

$$\kappa_s = \frac{\left(2ma_{0,0} + 2kb_{0,0}\right)\overline{\omega}^{n,m,l,k}_r(r_c)}{\hat{u}^{n,0,l,0}_r(r_c)} \tag{58}$$

The correction to the fundamentals is found by substitution back into equation (45).

2.5. About the Definition of the Amplitude

Changing the definitions of the amplitudes in equations (23) and (28) leaves the analysis essentially unchanged. Operationally, only the quantity $\overline{\omega}_r^{n,m,l,k}(r_c)/\hat{u}_r^{n,0,l,0}(r_c)$ in equation (58) needs to be changed. All the numerical computations up to the calculation of κ_s remain the same as long as the normalizations of the linear eigenfunctions in equations (24) and (29) are fixed. Hence, one can study the influence of different amplitude definitions on the Landau coefficients without repeating the bulk of the computations. (The equations to be solved for higher order Landau coefficients depend on the lower order Landau coefficients; so if higher order Landau coefficients are to be calculated, changing the amplitude definition would require recomputing many more solutions.) In this subsection, we make some observations regarding how the Landau coefficients vary with the amplitude definition and how this information can guide the use of the weakly nonlinear theory.

All valid definitions of the amplitudes tend toward the same Landau coefficients when the linear growth rates $a_{0,0}$ and $b_{0,0}$ tend toward zero. One can see this by following the approach of Watson (ref. 12) and expanding $\chi^1_{n,m,l,k}$ in equation (48) in powers of $2(ma_{0,0}+kb_{0,0})$ so that

$$\chi^1_{n,m,l,k} = \frac{1}{2(ma_{0,0}+kb_{0,0})}\,\chi^{1,-1}_{n,m,l,k} + \chi^{1,0}_{n,m,l,k} + 2(ma_{0,0}+kb_{0,0})\chi^{1,1}_{n,m,l,k} + \cdots \tag{59}$$

By equating like powers of $2(ma_{0,0}+kb_{0,0})$, we find that at leading order, $\chi^1_{n,m,l,k}(r)$ is proportional to the linear eigenfunction $\hat{\mathbf{q}}_{n,0,l,0}(r)$. Herbert (ref. 15) uses this in his proof that the Landau coefficients obtained with his method are the same as those obtained with the Watson method (ref. 12) as the neutral curve is approached. Varying the amplitude definition does not change the ratio $\overline{\omega}_r^{n,m,l,k}(r_c)/\hat{u}_r^{n,0,l,0}(r_c)$ in equation (58) if $\chi^1_{n,m,l,k}(r)$ is proportional to $\hat{\mathbf{q}}_{n,0,l,0}(r)$. Hence, for $2(ma_{0,0}+kb_{0,0}) \to 0$, the Landau coefficients become independent of amplitude definition.

When the quantity $2(ma_{0,0}+kb_{0,0})$ is not small, $\chi^1_{n,m,l,k}(r)$ is not approximately proportional to $\hat{\mathbf{q}}_{n,0,l,0}(r)$ and the Landau coefficients can depend strongly on the amplitude definition. Local amplitude definitions like the ones used above will generate Landau coefficients that describe the local behavior of the disturbance. Locally, parts of the disturbance can grow while other parts can decay; hence, the Landau coefficients corresponding to different amplitude definitions may not even have the same sign. As noted by Herbert (ref. 15) and others, the dependence of the Landau coefficients on the amplitude definition corresponds to a rearranging of the higher order terms in the infinite series. Large variations in the Landau coefficients as the amplitude definition is changed should warn the user of the theory that the higher order terms are likely to be important for the specific problem considered.

Because integration tends to smooth rapid local changes, amplitude definitions that measure global quantities are likely to be more reliable in predicting the overall behavior of the disturbance in these cases. Therefore, one useful alternative amplitude definition is a slight variation of one proposed by Herbert (ref. 15). Here,

$$A(t) = \left| \frac{\int_{r_i}^{r_o} \hat{\mathbf{q}}_{-1,0,0,0}(r) \cdot \tilde{\mathbf{q}}_{1,0}(r)\; dr}{\int_{r_i}^{r_o} \hat{\mathbf{q}}_{-1,0,0,0}(r) \cdot \hat{\mathbf{q}}_{1,0,0,0}(r)\; dr} \right| \tag{60}$$

with a corresponding definition for $B(t)$. Note that $\hat{\mathbf{q}}_{-1,0,0,0}$ is just the complex conjugate of $\hat{\mathbf{q}}_{1,0,0,0}$. The expression for the Landau coefficient is then changed from equation (58) to

$$\kappa_s = (2ma_{0,0}+2kb_{0,0})\,\frac{\int_{r_i}^{r_o} \hat{\mathbf{q}}_{-n,0,-l,0}(r) \cdot \chi^1_{n,m,l,k}(r)\; dr}{\int_{r_i}^{r_o} \hat{\mathbf{q}}_{-n,0,-l,0}(r) \cdot \hat{\mathbf{q}}_{n,0,l,0}(r)\; dr} \tag{61}$$

Note that the normalization of the linear eigenfunctions need not be changed.

Because DHZ and much of our early work used local amplitude definitions, comparisons will be somewhat simpler if we use a local amplitude definition. Unless otherwise specified, the results

reported here used equations (23) and (28) for the amplitudes and equations (24) and (29) for the eigenfunction normalizations.

2.6. Numerical Approach

All the equation systems are solved using a Chebyshev collocation procedure (ref. 20). The left-hand-side operators for all the systems (except the mean-flow corrections) are generated with a single subroutine. The operators for the mean-flow corrections need to ensure that only streamwise velocity perturbations are nonzero. This was most easily done using a separate subroutine. The right-hand-side vectors were sufficiently different from each other that it was more convenient to use MACSYMA to write individual subroutines for each of the equation systems. The two eigenproblems are solved first with a global solver to obtain the eigenvalue spectrum. The eigenvectors associated with the most unstable eigenvalue are obtained with a local iterative procedure. For $\lambda < 10^{-4}$ (which is the regime studied here), a straightforward evaluation of the mean flow using 64-bit precision leads to a substantial roundoff error; hence 128-bit precision was used for the calculation of the mean-flow profile. For the stability calculations, we found that 65 collocation points across the channel (including the end points) produced Landau coefficients that agreed to at least 3 digits with those obtained with 97 collocation points.

3. Results

3.1. Predictions of the Weakly Nonlinear Theory

We present some of our weakly nonlinear results in the context of nonlinear autonomous systems. Recall that A measures the amplitude of the TS wave and B that of the Dean disturbance. Equations (36) and (37) truncated at third order admit four possible steady-state solutions: the trivial solution, finite A with $B = 0$, finite B with $A = 0$, and a combined state with finite values of both A and B. Each of these states is a critical point and may be classified according to the local behavior of the solutions in its vicinity. In the phase plane (B versus A), stable nodes are identified as those for which solution trajectories near the point converge to the node, unstable nodes are critical points from which solution trajectories diverge, and saddle points are those points for which a finite number of trajectories converge to the point while all others diverge.

Several trajectories are illustrated in figure 2 for a case where $R = 6291.67$, $\lambda = 2.189 \times 10^{-5}$, $\aleph = 74257$, and $\beta = 4.51$. These parameters were used extensively by Singer and Zang (ref. 13) in their direct numerical simulations. An explicit fourth-order Runge- Kutta differencing scheme was used to trace the subsequent trajectories. The filled circles show the two stable equilibrium points at ($A = 3.8 \times 10^{-3}$, $B = 0$) and ($A = 0$, $B = 7.0 \times 10^{-5}$), respectively. Trajectories initiated near either of these points tend to converge to the respective nodes. The squares represent unstable nodes and saddle points. Two initial conditions start close to the saddle point at ($A = 2.4 \times 10^{-4}$, $B = 3.5 \times 10^{-5}$) and go to different stable equilibrium states. The flow is especially sensitive to small changes near the saddle point. The unstable node at the origin is the end point of a semi-infinite curve that goes through the saddle point, and separates the region of attraction of the two stable nodes. Quite different behavior can be obtained depending upon the initial values of A and B.

A slightly different scenario exists when we consider $R = 5000$, $\lambda = 2.179 \times 10^{-5}$, $\aleph = 10^5$, and $\beta = 2.0$. In figure 3, pairs of trajectories with initial values of A differing by 0.001 are plotted for various initial values of B. In many ways, the qualitative behavior seen here is similar to that illustrated in figure 2. The origin is an unstable node, there is a saddle point with nonzero A and B, and there is a stable node with nonzero B but $A = 0$. A semi-infinite curve extends from the origin, goes through the saddle point, and separates the domain into a region that is attracted to the stable node with ($A = 0$, $B = 7.7 \times 10^{-4}$) and a region in which $A \to \infty$. This shows how important the nonlinear interaction can be. Without a Dean disturbance, the TS wave has unbounded growth; however, the inclusion of an additional disturbance at sufficiently large amplitude can completely stabilize the otherwise growing TS wave.

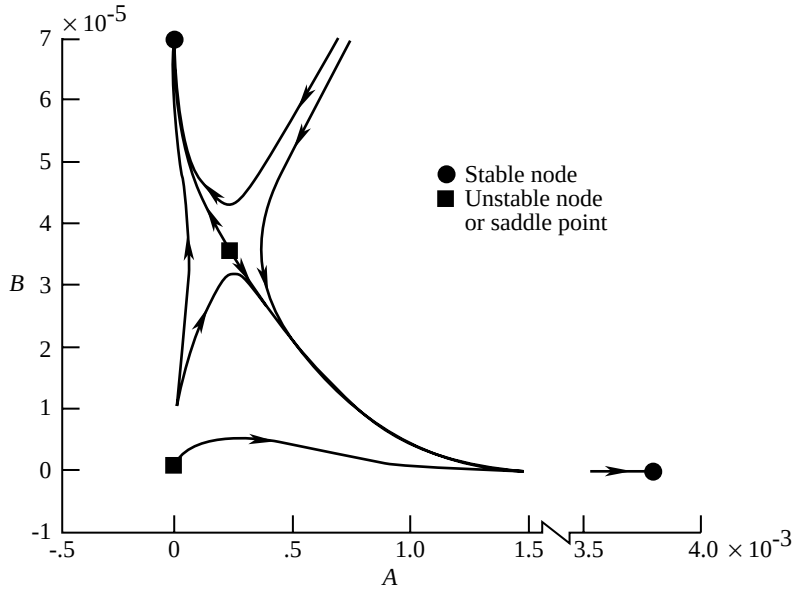

Figure 2. Trajectories in phase space with $R = 6291.67, \lambda = 2.189 \times 10^{-5}, \aleph = 74\,257$, and $\beta = 4.51$.

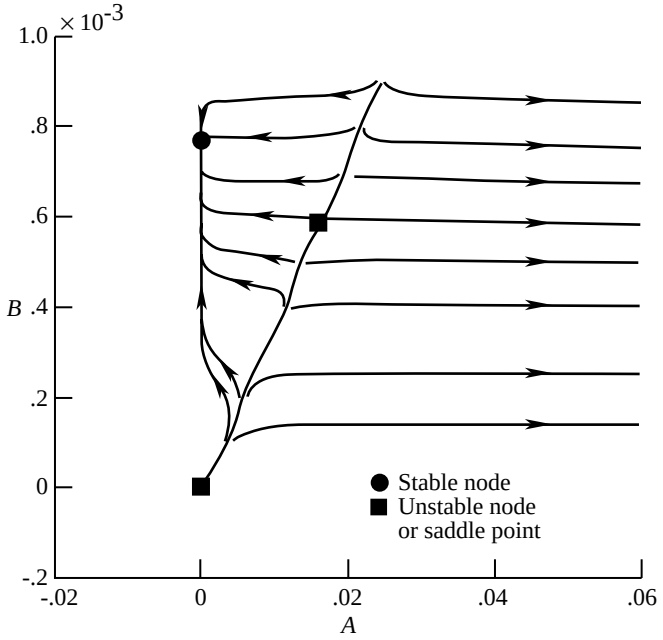

Figure 3. Trajectories in phase space with $R = 5000, \lambda = 2.179 \times 10^{-5}, \aleph = 10^5$, and $\beta = 2.0$.

3.2. Comparison With Direct Numerical Simulation

Here we will compare the results of our weakly nonlinear analysis with those obtained by DNS.

The numerical simulation code (ref. 13) uses a curved channel variant of the method described by Zang and Hussaini (ref. 21) with the nonlinear terms in skew-symmetric form (ref. 22). Table 2 reports the least stable eigenvalues ($a_{0,0} - ig_{0,0}$) obtained with a spectral linear stability code and the corresponding results of DNS with two different time steps. (Note that in this context $\aleph$ and β refer to the azimuthal and axial wave numbers of the linear waves.) Sixty-five points across the channel are used. Data from the DNS are taken after 100 time steps. Using a time step $\Delta t = 0.0001$, the complex growth rates differ from those predicted by linear theory by less than 1 part in 10^4. In the simulations reported below, we are primarily concerned with long-time trends and final steady-state solutions; hence, the additional time advancement errors associated with the larger time step,

$\Delta t = 0.01$, are not expected to be important. The larger time step gives a maximum Courant (CFL) number of 0.01, still well within the numerically stable regime. Additional details of code validation studies in both the linear and nonlinear regimes are given by Singer and Zang (ref. 13).

Table 2. Comparison of Linear Growth Rates

[All values are multiplied by 10^4]

R	$\aleph$	β	Linear stability	DNS with $\Delta t = 0.01$	DNS with $\Delta t = 0.0001$
5 000	10^5	0	$3.1189 - 4236.9i$	$3.0736 - 4241.8i$	$3.1185 - 4236.9i$
5 000	0	2.0	$6.6331 + 0i$	$6.6336 + 0i$	$6.6335 + 0i$
5 000	10^5	2.0	$-138.2126 - 16\,214.8i$	$-138.2154 - 16\,214.8i$	$-138.2126 - 16\,214.8i$
10 000	80 000	0	$86.4287 - 2709.1i$	$86.4204 - 2709.4i$	$86.4291 - 2709.1i$
10 000	0	3.0	$21.5591 + 0i$	$21.5599 + 0i$	$21.5599 + 0i$
10 000	80 000	3.0	$-90.6119 - 12\,993.3i$	$-90.6131 - 12\,993.3i$	$-90.6119 - 12\,993.3i$

Sufficient spatial resolution in the simulation can be ensured by using the guideline suggested by Krist and Zang (ref. 23). They suggest that "grid refinement is needed in any direction where the tail of the energy spectrum reaches 10^{-8} of the low-frequency value." This guarantees that truncation errors in the velocity will be less than 0.01 percent. Such detailed resolution is not necessary for the purposes of these simulations. We have found that the high wave number end of the energy spectrum could be as much as 10^{-4} of the low wave number value and still provide results similar to those obtained when the Krist and Zang guideline was strictly followed. The relative insensitivity to resolution is attributed to the rather minor role that small scales play in the present wave-interaction problem.

We have simulated four cases with $R = 6291.67$, $\lambda = 2.189 \times 10^{-5}$, $\aleph = 74\,257$, and $\beta = 4.51$. The predictions of the weakly nonlinear theory for these cases were discussed above in conjunction with figure 2.

In the first case, only a Dean disturbance is included in the initial conditions. The weakly nonlinear theory suggests that an equilibrium state with $B = 7.0 \times 10^{-5}$ develops corresponding to a maximum streamwise velocity perturbation of 5.84 percent of $\overline{U}^*$. We have initiated the simulation with the Dean linear eigenfunction having an initial strength, $B = 6.95 \times 10^{-5}$. At $t = 3.4845 \times 10^4$, the magnitude of the instantaneous growth rate has decreased by more than a factor of 100 and the simulation is stopped with $B = 6.7 \times 10^{-5}$. In this case, the difference between the equilibrium state predicted by the weakly nonlinear theory and that obtained from the DNS is less than 5 percent.

In the second case, only a TS wave with initial amplitude $A = 3.5 \times 10^{-3}$ is included. The weakly nonlinear theory predicts a TS equilibrium state with $A = 3.8 \times 10^{-3}$, resulting in a maximum streamwise disturbance of 1.94 percent of $\overline{U}^*$. The DNS is stopped at a time $t = 1.1367 \times 10^4$ corresponding to over 480 TS wave periods. At this time, $A = 4.0 \times 10^{-3}$. The difference between theory and DNS is 5 percent.

The remaining two simulations with these parameters include both Dean and TS perturbations in the initial conditions. In both cases we have initiated the Dean disturbances with $B = 6.95 \times 10^{-5}$. This value is slightly less than the equilibrium amplitude that we obtained in case 1.

When the initial strength of the TS disturbance is $A = 2.94 \times 10^{-4}$, the weakly nonlinear phase-plane diagram in figure 2 shows that the disturbances are in a region of attraction of the saturated Dean vortex. Here the TS wave is expected to decay and the Dean vortex should grow

to its equilibrium state. In figure 4 we plot the amplitude of both the Dean and TS disturbances, normalized by their respective amplitudes at time $t = 0$. The long-time prediction of the weakly nonlinear theory agrees with the results of the DNS.

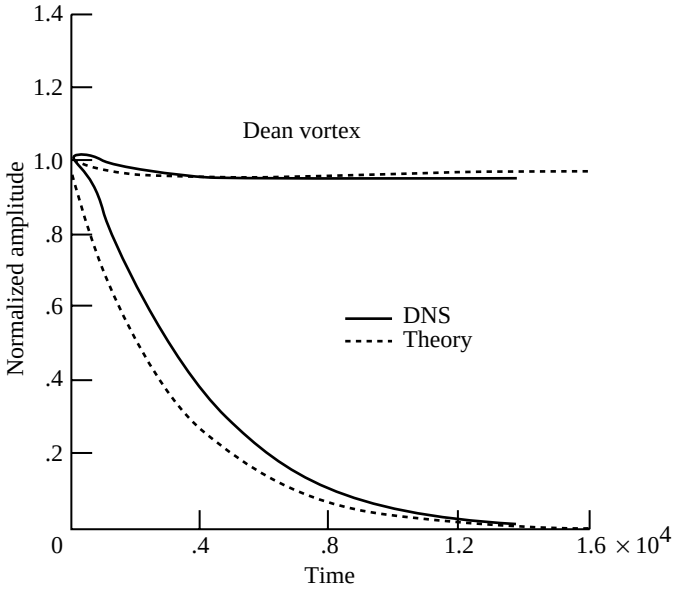

Figure 4. Time evolution of TS and Dean disturbances for $R = 6291.67, \lambda = 2.189 \times 10^{-5}, \aleph = 74\,257$, and $\beta = 4.51$. The initial TS disturbance has $A = 2.7 \times 10^{-4}$; the initial Dean disturbance has $B = 7.0 \times 10^{-5}$.

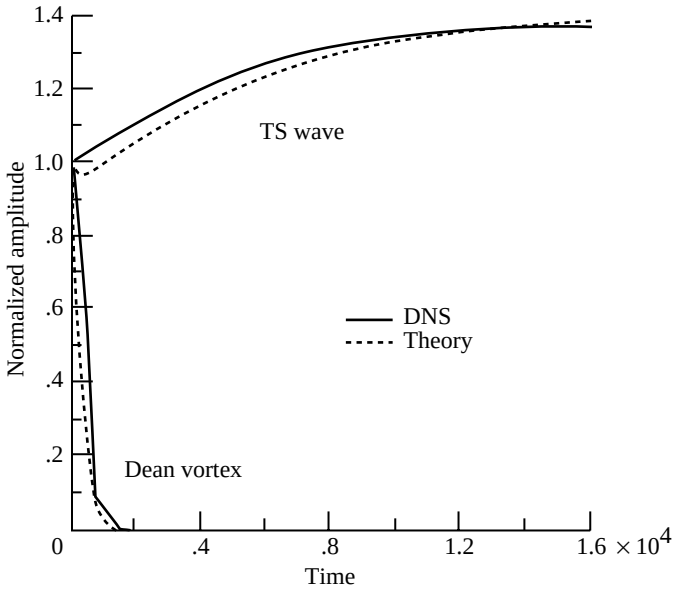

Figure 5. Time evolution of TS and Dean disturbances for $R = 6291.67, \lambda = 2.189 \times 10^{-5}, \aleph = 74\,257$, and $\beta = 4.51$. The initial TS disturbance has $A = 2.7 \times 10^{-3}$; the initial Dean disturbance has $B = 7.0 \times 10^{-5}$.

For a stronger TS disturbance ($A = 2.94 \times 10^{-3}$), the disturbances are in a region of attraction of the saturated TS wave. Figure 5 shows the amplitude histories for this case. Here it is the TS wave that grows toward its equilibrium value and the Dean disturbance that experiences rapid decay. Again the weakly nonlinear theory and the DNS agree.

Similar comparisons are made with $R = 5000$, $\lambda = 2.179 \times 10^{-5}$, $\aleph = 10^5$, and $\beta = 2.0$. The predictions of the weakly nonlinear theory for this set of parameters are summarized in figure 3.

A numerical simulation initiated with $A = 2 \times 10^{-3}$ and $B = 0$ confirmed that the amplitude A increased with increasing growth rate, at least until $A = 4.8 \times 10^{-3}$ when the simulation was terminated.

A Dean vortex alone in this flow is predicted to reach an equilibrium state with $B = 7.7 \times 10^{-4}$. This value of B corresponds to a maximum streamwise velocity perturbation that is 62.4 percent of the undisturbed laminar bulk velocity. Using this as an initial amplitude, an equilibrium state with $B = 4.3 \times 10^{-4}$ is obtained in the direct numerical simulations. The difference between the DNS result and that of the weakly nonlinear theory is not unexpected since the disturbance amplitudes are so large. In addition, in this case the Landau coefficients $b_{1,0}$ and $b_{0,1}$ are quite sensitive to the amplitude definition. This warns us to temper our expectations from the theory for these parameter values.

The final simulation performed used initial values of A and B as $A = 2 \times 10^{-3}$ and $B = 6.5 \times 10^{-4}$. In this case, the weakly nonlinear theory predicts that the TS wave will decay, leaving only a Dean disturbance in the flow. The time evolutions of the TS and Dean disturbances are plotted in figure 6 through $t = 0.5 \times 10^3$. Though the simulation was terminated before a steady-state solution was reached, the prediction of the weakly nonlinear theory is qualitatively supported. After the initial transient, the TS wave decays rapidly. Considering the large amplitude disturbances in the flow, the theory and the simulation agree well.

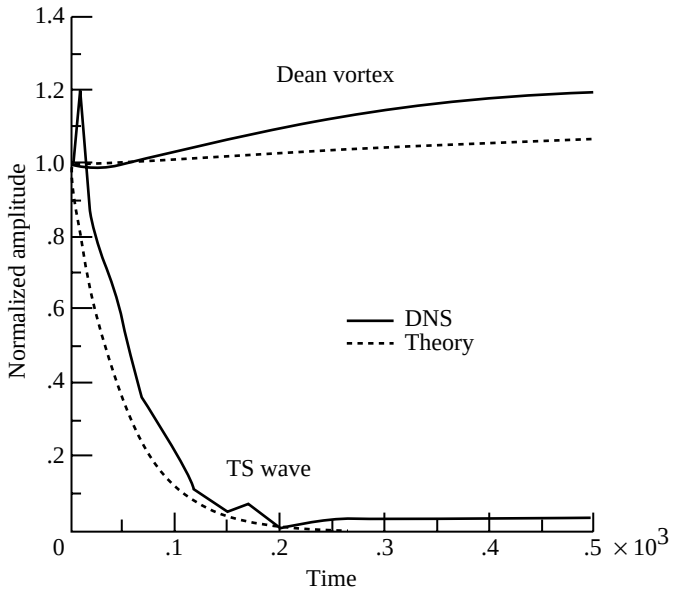

Figure 6. Time evolution of TS and Dean disturbances for $R = 5000, \lambda = 2.179 \times 10^{-5}, \aleph = 10^5$, and $\beta = 2.0$. The initial TS disturbance has $A = 2.0 \times 10^{-3}$; the initial Dean disturbance has $B = 6.5 \times 10^{-4}$.

3.3. Comparison With Previous Theory

In this subsection we compare our Landau coefficients with those of DHZ for two specific cases for which normalized Landau coefficients are available in table 1 of reference 10. Using our nondimensionalizations, the Landau constants from the current theory and from the theory of DHZ are shown in tables 3 and 4. The parameters of table 3 were studied extensively by Singer and Zang (ref. 13) and are discussed above. The quantities $a_{0,0}$ and $b_{0,0}$ from DHZ were taken directly from their linear eigenvalue solver, rather than by perturbing away from the neutral stability curve. Except for the coefficient $b_{1,0}$, which represents the effect of the TS wave on the Dean disturbance, the coefficients show satisfactory agreement. For the cases considered here, the variation in $b_{1,0}$ with various amplitude definitions is not large enough to explain the discrepancy. Singer and Zang (ref. 13) suggested that a yet-unknown error in DHZ led to erroneous values of $b_{1,0}$. Our work here supports that suggestion.

Table 3. Comparison of Landau Coefficients for $R = 6291.67, \lambda = 2.189 \times 10^{-5}$, $\aleph = 74\,257$, and $\beta = 4.508$

Theory	$a_{0,0}$	$a_{1,0}$	$a_{0,1}$	$b_{0,0}$	$b_{1,0}$	$b_{0,1}$
Current	1.21×10^{-4}	-8.25	$-95\,000$	3.97×10^{-5}	-482	-7640
DHZ	1.20×10^{-4}	-8.85	$-101\,000$	3.97×10^{-5}	1.23×10^{5}	-8470

Table 4. Comparison of Landau Coefficients for $R = 4175, \lambda = 2.179 \times 10^{-5}$, $\aleph = 86\,800$, and $\beta = 2.76$

Theory	$a_{0,0}$	$a_{1,0}$	$a_{0,1}$	$b_{0,0}$	$b_{1,0}$	$b_{0,1}$
Current	1.18×10^{-5}	3.97	$-46\,600$	7.66×10^{-6}	-233	-3340
DHZ	1.33×10^{-5}	3.97	$-46\,900$	7.66×10^{-6}	1.44	-3390

4. Concluding Remarks

We have presented a weakly nonlinear theory to describe interactions between Tollmien-Schlichting (TS) waves and Dean vortices in curved channel flow. The approach used to calculate the Landau coefficients is an extension of that developed by Herbert. This approach provides not only the Landau coefficients but also the shape change of the fundamental disturbances with amplitude. We also discussed the effects of amplitude definition on the Landau coefficients.

The analysis indicates that the resultant flow can be quite sensitive to the details of the initial conditions. By the addition of a Dean vortex of relatively small amplitude, one can change the long-time evolution of the flow dramatically. In one case we observed a switching of the equilibrium solution from a finite-amplitude TS wave with no Dean vortex to a finite-amplitude Dean vortex with no TS wave. A more dramatic change occurred in another case where a TS wave alone in the flow would have grown ad infinitum, but the presence of a Dean vortex caused the TS wave to decay and the Dean vortex then evolved toward an equilibrium state.

Direct numerical simulations verify the predictions of the theory. When the amplitudes of the disturbances are not too large, the direct numerical simulations and the weakly nonlinear theory agree quite well. When the amplitudes of the disturbances are large (on the order of 60 percent of the centerline velocity), the simulations and the theory still qualitatively agree.

A comparison of our results with those of Daudpota, Hall, and Zang (DHZ), who also developed a similar weakly nonlinear theory, indicates that DHZ have an error in the computation of one of their Landau coefficients.

NASA Langley Research Center
Hampton, VA 23665-5225
January 9, 1992

5. Appendix A

The Left-Hand-Side Operator $\mathbf{L}_{n,l}$

The elements of the operator $\mathbf{L}_{n,l}$ are given as

$$\mathbf{L}_{n,l} = \begin{pmatrix} L^{1,1} & L^{1,2} & L^{1,3} & L^{1,4} \\ L^{2,1} & L^{2,2} & L^{2,3} & L^{2,4} \\ L^{3,1} & L^{3,2} & L^{3,3} & L^{3,4} \\ L^{4,1} & L^{4,2} & L^{4,3} & L^{4,4} \end{pmatrix}$$

$$L^{1,1} = i\aleph\frac{1}{r}U_\theta + \frac{1}{R}\left(l^2\beta^2 + \frac{n^2\aleph^2+1}{r^2} - \frac{1}{r}\frac{d}{dr} - \frac{d^2}{dr^2}\right)$$

$$L^{1,2} = -2\frac{U_\theta}{r} + \frac{2in\aleph}{r^2R}$$

$$L^{1,3} = 0$$

$$L^{1,4} = \frac{d}{dr}$$

$$L^{2,1} = \frac{dU_\theta}{dr} + \frac{U_\theta}{r} - \frac{2in\aleph}{r^2R}$$

$$L^{2,2} = i\aleph\frac{1}{r}U_\theta + \frac{1}{R}\left(l^2\beta^2 + \frac{n^2\aleph^2+1}{r^2} - \frac{1}{r}\frac{d}{dr} - \frac{d^2}{dr^2}\right)$$

$$L^{2,3} = 0$$

$$L^{2,4} = i\frac{n\aleph}{r}$$

$$L^{3,1} = 0$$

$$L^{3,2} = 0$$

$$L^{3,3} = i\aleph\frac{1}{r}U_\theta + \frac{1}{R}\left(l^2\beta^2 + \frac{n^2\aleph^2}{r^2} - \frac{1}{r}\frac{d}{dr} - \frac{d^2}{dr^2}\right)$$

$$L^{3,4} = il\beta$$

$$L^{4,1} = \frac{1}{r} + \frac{d}{dr}$$

$$L^{4,2} = i\frac{n\aleph}{r}$$

$$L^{4,3} = il\beta$$

$$L^{4,4} = 0$$

6. Appendix B

The Right-Hand-Side Vectors $\mathbf{R}_s$

The elements of the right-hand-side vectors $\mathbf{R}_s$ are given explicitly as

$$\mathbf{R}_s = \begin{pmatrix} R_s^1 \\ R_s^2 \\ R_s^3 \\ R_s^4 \end{pmatrix}$$

Equation system $s = 5$ corresponds to the TS harmonic. Its right-hand-side vector is given by

$$R_5^1 = -(i\aleph \hat{u}_\theta^{1,0,0,0} \hat{u}_r^{1,0,0,0})/r + (\hat{u}_\theta^{1,0,0,0})^2/r - \frac{d}{dr}(\hat{u}_r^{1,0,0,0})\ \hat{u}_r^{1,0,0,0}$$

$$R_5^2 = -i\aleph(\hat{u}_\theta^{1,0,0,0})^2/r - (\hat{u}_\theta^{1,0,0,0} \hat{u}_r^{1,0,0,0})/r - \frac{d}{dr}(\hat{u}_\theta^{1,0,0,0})\ \hat{u}_r^{1,0,0,0}$$

$$R_5^3 = -(i\aleph \hat{u}_\theta^{1,0,0,0} \hat{u}_z^{1,0,0,0})/r + \hat{u}_r^{1,0,0,0} \frac{d}{dr}(\hat{u}_z^{1,0,0,0})$$

$$R_5^4 = 0$$

Equation system $s = 6$ corresponds to the Dean harmonic. Its right-hand-side vector is given by

$$R_6^1 = -i\beta \hat{u}_z^{0,0,1,0} \hat{u}_r^{0,0,1,0} + (\hat{u}_\theta^{0,0,1,0})^2/r - \frac{d}{dr}(\hat{u}_r^{0,0,1,0})\ \hat{u}_r^{0,0,1,0}$$

$$R_6^2 = -i\beta \hat{u}_\theta^{0,0,1,0} \hat{u}_z^{0,0,1,0} - (\hat{u}_\theta^{0,0,1,0} \hat{u}_r^{0,0,1,0})/r - \frac{d}{dr}(\hat{u}_\theta^{0,0,1,0})\ \hat{u}_r^{0,0,1,0}$$

$$R_6^3 = -i\beta(\hat{u}_z^{0,0,1,0})^2 + \hat{u}_r^{0,0,1,0} \frac{d}{dr}(\hat{u}_z^{0,0,1,0})$$

$$R_6^4 = 0$$

Equation system $s = 7$ corresponds to the product of the TS and Dean fundamentals. Its right-hand-side vector is given by

$$R_7^1 = -(i\aleph \hat{u}_\theta^{0,0,1,0} \hat{u}_r^{1,0,0,0})/r - i\beta \hat{u}_r^{0,0,1,0} \hat{u}_z^{1,0,0,0} + (2\hat{u}_\theta^{0,0,1,0} \hat{u}_\theta^{1,0,0,0})/r$$
$$- \left[\frac{d}{dr}(\hat{u}_r^{0,0,1,0})\ \hat{u}_r^{1,0,0,0} + \frac{d}{dr}(\hat{u}_r^{1,0,0,0})\ \hat{u}_r^{0,0,1,0}\right]$$

$$R_7^2 = -(i\aleph \hat{u}_\theta^{0,0,1,0} \hat{u}_\theta^{1,0,0,0})/r - i\beta \hat{u}_\theta^{0,0,1,0} \hat{u}_z^{1,0,0,0} - (\hat{u}_\theta^{0,0,1,0} \hat{u}_r^{1,0,0,0} + \hat{u}_\theta^{1,0,0,0} \hat{u}_r^{0,0,1,0})/r$$
$$- \left[\frac{d}{dr}(\hat{u}_\theta^{0,0,1,0})\ \hat{u}_r^{1,0,0,0} + \frac{d}{dr}(\hat{u}_\theta^{1,0,0,0})\ \hat{u}_r^{0,0,1,0}\right]$$

$$R_7^3 = -(i\aleph \hat{u}_\theta^{0,0,1,0} \hat{u}_z^{1,0,0,0})/r - i\beta \hat{u}_z^{0,0,1,0} \hat{u}_z^{1,0,0,0} - \left[\frac{d}{dr}(\hat{u}_z^{0,0,1,0})\ \hat{u}_r^{1,0,0,0} + \frac{d}{dr}(\hat{u}_z^{1,0,0,0})\ \hat{u}_r^{0,0,1,0}\right]$$

$$R_7^4 = 0$$

Equation system $s = 8$ corresponds to the product of the TS fundamental and the complex conjugate of the Dean fundamental. Its right-hand-side vector is given by

$$
\begin{aligned}
R_8^1 &= -(i\aleph \hat{u}_\theta^{0,0,-1,0}\hat{u}_r^{1,0,0,0})/r + i\beta\hat{u}_r^{0,0,-1,0}\hat{u}_z^{1,0,0,0} + (2\hat{u}_\theta^{0,0,-1,0}\hat{u}_\theta^{1,0,0,0})/r \\
&\quad - \left[\frac{d}{dr}(\hat{u}_r^{0,0,-1,0})\ \hat{u}_r^{1,0,0,0} + \frac{d}{dr}(\hat{u}_r^{1,0,0,0})\ \hat{u}_r^{0,0,-1,0}\right] \\
R_8^2 &= -(i\aleph \hat{u}_\theta^{0,0,-1,0}\hat{u}_\theta^{1,0,0,0})/r + i\beta\hat{u}_\theta^{0,0,-1,0}\hat{u}_z^{1,0,0,0} - (\hat{u}_\theta^{0,0,-1,0}\hat{u}_r^{1,0,0,0} + \hat{u}_\theta^{1,0,0,0}\hat{u}_r^{0,0,-1,0})/r \\
&\quad - \left[\frac{d}{dr}(\hat{u}_\theta^{0,0,-1,0})\ \hat{u}_r^{1,0,0,0} + \frac{d}{dr}(\hat{u}_\theta^{1,0,0,0})\ \hat{u}_r^{0,0,-1,0}\right] \\
R_8^3 &= -(i\aleph \hat{u}_\theta^{0,0,-1,0}\hat{u}_z^{1,0,0,0})/r + i\beta\hat{u}_z^{0,0,-1,0}\hat{u}_z^{1,0,0,0} \\
&\quad - \left[\frac{d}{dr}(\hat{u}_z^{0,0,-1,0})\ \hat{u}_r^{1,0,0,0} + \frac{d}{dr}(\hat{u}_z^{1,0,0,0})\ \hat{u}_r^{0,0,-1,0}\right] \\
R_8^4 &= 0
\end{aligned}
$$

Equation system $s = 9$ corresponds to the self-correction of the TS fundamental. Its right-hand-side vector is given by

$$
\begin{aligned}
R_9^1 &= -i\aleph(2\hat{u}_\theta^{-1,0,0,0}\hat{u}_r^{2,0,0,0} + \hat{u}_\theta^{0,1,0,0}\hat{u}_r^{1,0,0,0} - \hat{u}_\theta^{2,0,0,0}\hat{u}_r^{-1,0,0,0})/r \\
&\quad + (2\hat{u}_\theta^{-1,0,0,0}\hat{u}_\theta^{2,0,0,0} + 2\hat{u}_\theta^{0,1,0,0}\hat{u}_\theta^{1,0,0,0})/r \\
&\quad - \left[\frac{d}{dr}(\hat{u}_r^{2,0,0,0})\ \hat{u}_r^{-1,0,0,0} + \frac{d}{dr}(\hat{u}_r^{-1,0,0,0})\ \hat{u}_r^{2,0,0,0} + \frac{d}{dr}(\hat{u}_r^{0,1,0,0})\ \hat{u}_r^{1,0,0,0} + \frac{d}{dr}(\hat{u}_r^{1,0,0,0})\ \hat{u}_r^{0,1,0,0}\right] \\
&\quad - (a_{1,0} - ig_{1,0})\ \hat{u}_r^{1,0,0,0} \\
R_9^2 &= -i\aleph(\hat{u}_\theta^{-1,0,0,0}\hat{u}_\theta^{2,0,0,0} + \hat{u}_\theta^{0,1,0,0}\hat{u}_\theta^{1,0,0,0})/r \\
&\quad - (\hat{u}_\theta^{-1,0,0,0}\hat{u}_r^{2,0,0,0} + \hat{u}_\theta^{2,0,0,0}\hat{u}_r^{-1,0,0,0} + \hat{u}_\theta^{0,1,0,0}\hat{u}_r^{1,0,0,0} + \hat{u}_\theta^{1,0,0,0}\hat{u}_r^{0,1,0,0})/r \\
&\quad - \left[\frac{d}{dr}(\hat{u}_\theta^{-1,0,0,0})\ \hat{u}_r^{2,0,0,0} + \frac{d}{dr}(\hat{u}_\theta^{2,0,0,0})\ \hat{u}_r^{-1,0,0,0} + \frac{d}{dr}(\hat{u}_\theta^{0,1,0,0})\ \hat{u}_r^{1,0,0,0} + \frac{d}{dr}(\hat{u}_\theta^{1,0,0,0})\ \hat{u}_r^{0,1,0,0}\right] \\
&\quad - (a_{1,0} - ig_{1,0})\ \hat{u}_\theta^{1,0,0,0} \\
R_9^3 &= -i\aleph(2\hat{u}_\theta^{-1,0,0,0}\hat{u}_z^{2,0,0,0} + \hat{u}_\theta^{0,1,0,0}\hat{u}_z^{1,0,0,0} - \hat{u}_\theta^{2,0,0,0}\hat{u}_z^{-1,0,0,0})/r \\
&\quad - \left[\frac{d}{dr}(\hat{u}_z^{-1,0,0,0})\ \hat{u}_r^{2,0,0,0} + \frac{d}{dr}(\hat{u}_z^{2,0,0,0})\ \hat{u}_r^{-1,0,0,0} + \frac{d}{dr}(\hat{u}_z^{0,1,0,0})\ \hat{u}_r^{1,0,0,0} + \frac{d}{dr}(\hat{u}_z^{1,0,0,0})\ \hat{u}_r^{0,1,0,0}\right] \\
&\quad - (a_{1,0} - ig_{1,0})\ \hat{u}_z^{1,0,0,0} \\
R_9^4 &= 0
\end{aligned}
$$

Equation system $s = 10$ corresponds to the self-correction of the Dean fundamental. Its right-hand-side vector is given by

$$
\begin{aligned}
R^1_{10} = & -i\beta(2\hat{u}_z^{0,0,-1,0}\hat{u}_r^{0,0,2,0} + \hat{u}_z^{0,0,0,1}\hat{u}_r^{0,0,1,0} - \hat{u}_z^{0,0,2,0}\hat{u}_r^{0,0,-1,0}) \\
& + (2\hat{u}_\theta^{0,0,-1,0}\hat{u}_\theta^{0,0,2,0} + 2\hat{u}_\theta^{0,0,0,1}\hat{u}_\theta^{0,0,1,0})/r \\
& - \left[\frac{d}{dr}(\hat{u}_r^{0,0,2,0})\ \hat{u}_r^{0,0,-1,0} + \frac{d}{dr}(\hat{u}_r^{0,0,-1,0})\hat{u}_r^{0,0,2,0} + \frac{d}{dr}(\hat{u}_r^{0,0,0,1})\ \hat{u}_r^{0,0,1,0} + \frac{d}{dr}(\hat{u}_r^{0,0,1,0})\ \hat{u}_r^{0,0,0,1}\right] \\
& - (b_{0,1} - ih_{0,1})\ \hat{u}_r^{0,0,1,0} \\
R^2_{10} = & -i\beta(2\hat{u}_\theta^{0,0,2,0}\hat{u}_z^{0,0,-1,0} + \hat{u}_\theta^{0,0,1,0}\hat{u}_z^{0,0,0,1} - \hat{u}_\theta^{0,0,-1,0}\hat{u}_z^{0,0,2,0}) \\
& - (\hat{u}_\theta^{0,0,-1,0}\hat{u}_r^{0,0,2,0} + \hat{u}_\theta^{0,0,2,0}\hat{u}_r^{0,0,-1,0} + \hat{u}_\theta^{0,0,0,1}\hat{u}_r^{0,0,1,0} + \hat{u}_\theta^{0,0,1,0}\hat{u}_r^{0,0,0,1})/r \\
& - \left[\frac{d}{dr}(\hat{u}_\theta^{0,0,-1,0})\ \hat{u}_r^{0,0,2,0} + \frac{d}{dr}(\hat{u}_\theta^{0,0,2,0})\ \hat{u}_r^{0,0,-1,0} + \frac{d}{dr}(\hat{u}_\theta^{0,0,0,1})\ \hat{u}_r^{0,0,1,0} + \frac{d}{dr}(\hat{u}_\theta^{0,0,1,0})\ \hat{u}_r^{0,0,0,1}\right] \\
& - (b_{0,1} - ih_{0,1})\ \hat{u}_\theta^{0,0,1,0} \\
R^3_{10} = & -i\beta(\hat{u}_z^{0,0,-1,0}\hat{u}_z^{0,0,2,0} + \hat{u}_z^{0,0,0,1}\hat{u}_z^{0,0,1,0}) \\
& - \left[\frac{d}{dr}(\hat{u}_z^{0,0,-1,0})\ \hat{u}_r^{0,0,2,0} + \frac{d}{dr}(\hat{u}_z^{0,0,2,0})\ \hat{u}_r^{0,0,-1,0} + \frac{d}{dr}(\hat{u}_z^{0,0,0,1})\ \hat{u}_r^{0,0,1,0} + \frac{d}{dr}(\hat{u}_z^{0,0,1,0})\ \hat{u}_r^{0,0,0,1}\right] \\
& - (b_{0,1} - ih_{0,1})\ \hat{u}_z^{0,0,1,0} \\
R^4_{10} = & \ 0
\end{aligned}
$$

Equation system $s = 11$ corresponds to the correction of the TS fundamental by the Dean vortex. Its right-hand-side vector is given by

$$
\begin{aligned}
R^1_{11} = & -i\aleph\hat{u}_\theta^{0,0,-1,0}\hat{u}_r^{1,0,1,0} + \hat{u}_\theta^{0,0,0,1}\hat{u}_r^{1,0,0,0} + \hat{u}_\theta^{0,0,1,0}\hat{u}_r^{1,0,-1,0})/r \\
& + i\beta(\hat{u}_r^{0,0,-1,0}\hat{u}_z^{1,0,1,0} - \hat{u}_r^{0,0,1,0}\hat{u}_z^{1,0,-1,0} + \hat{u}_r^{1,0,-1,0}\hat{u}_z^{0,0,1,0} - \hat{u}_r^{1,0,1,0}\hat{u}_z^{0,0,-1,0}) \\
& + 2(\hat{u}_\theta^{0,0,-1,0}\hat{u}_\theta^{1,0,1,0} + \hat{u}_\theta^{0,0,0,1}\hat{u}_\theta^{1,0,0,0} + \hat{u}_\theta^{0,0,1,0}\hat{u}_\theta^{1,0,-1,0})/r \\
& - \left[\frac{d}{dr}(\hat{u}_r^{0,0,-1,0})\ \hat{u}_r^{1,0,1,0} + \frac{d}{dr}(\hat{u}_r^{0,0,0,1})\ \hat{u}_r^{1,0,0,0} + \frac{d}{dr}(\hat{u}_r^{0,0,1,0})\ \hat{u}_r^{1,0,-1,0} + \frac{d}{dr}(\hat{u}_r^{1,0,-1,0})\ \hat{u}_r^{0,0,1,0}\right. \\
& \left. + \frac{d}{dr}(\hat{u}_r^{1,0,0,0})\ \hat{u}_r^{0,0,0,1} + \frac{d}{dr}(\hat{u}_r^{1,0,1,0})\ \hat{u}_r^{0,0,-1,0}\right] - (a_{0,1} - ig_{0,1})\ \hat{u}_r^{1,0,0,0} \\
R^2_{11} = & -i\aleph(\hat{u}_\theta^{0,0,-1,0}\hat{u}_\theta^{1,0,1,0} + \hat{u}_\theta^{0,0,0,1}\hat{u}_\theta^{1,0,0,0} + \hat{u}_\theta^{0,0,1,0}\hat{u}_\theta^{1,0,-1,0})/r \\
& + i\beta(\hat{u}_\theta^{0,0,-1,0}\hat{u}_z^{1,0,1,0} - \hat{u}_\theta^{0,0,1,0}\hat{u}_z^{1,0,-1,0} + \hat{u}_\theta^{1,0,-1,0}\hat{u}_z^{0,0,1,0} - \hat{u}_\theta^{1,0,1,0}\hat{u}_z^{0,0,-1,0}) \\
& - (\hat{u}_\theta^{0,0,-1,0}\hat{u}_r^{1,0,1,0} + \hat{u}_\theta^{0,0,0,1}\hat{u}_r^{1,0,0,0} + \hat{u}_\theta^{0,0,1,0}\hat{u}_r^{1,0,-1,0} + \hat{u}_\theta^{1,0,-1,0}\hat{u}_r^{0,0,1,0} \\
& + \hat{u}_\theta^{1,0,0,0}\hat{u}_r^{0,0,0,1} + \hat{u}_\theta^{1,0,1,0}\hat{u}_r^{0,0,-1,0})/r \\
& - \left[\frac{d}{dr}(\hat{u}_\theta^{0,0,-1,0})\ \hat{u}_r^{1,0,1,0} + \frac{d}{dr}(\hat{u}_\theta^{0,0,0,1})\ \hat{u}_r^{1,0,0,0} + \frac{d}{dr}(\hat{u}_\theta^{0,0,1,0})\ \hat{u}_r^{1,0,-1,0} + \frac{d}{dr}(\hat{u}_\theta^{1,0,-1,0})\ \hat{u}_r^{0,0,1,0}\right. \\
& \left. + \frac{d}{dr}(\hat{u}_\theta^{1,0,0,0})\ \hat{u}_r^{0,0,0,1} + \frac{d}{dr}(\hat{u}_\theta^{1,0,1,0})\ \hat{u}_r^{0,0,-1,0}\right] - (a_{0,1} - ig_{0,1})\ \hat{u}_\theta^{1,0,0,0}
\end{aligned}
$$

$$R_{11}^3 = -i\aleph(\hat{u}_\theta^{0,0,-1,0}\hat{u}_z^{1,0,1,0} + \hat{u}_\theta^{0,0,0,1}\hat{u}_z^{1,0,0,0} + \hat{u}_\theta^{0,0,1,0}\hat{u}_z^{1,0,-1,0})/r$$
$$- \left[\frac{d}{dr}(\hat{u}_z^{0,0,-1,0})\ \hat{u}_r^{1,0,1,0} + \frac{d}{dr}(\hat{u}_z^{0,0,0,1})\ \hat{u}_r^{1,0,0,0} + \frac{d}{dr}(\hat{u}_z^{0,0,1,0})\ \hat{u}_r^{1,0,-1,0} + \frac{d}{dr}(\hat{u}_z^{1,0,-1,0})\ \hat{u}_r^{0,0,1,0}\right.$$
$$\left. + \frac{d}{dr}(\hat{u}_z^{1,0,0,0})\ \hat{u}_r^{0,0,0,1} + \frac{d}{dr}(\hat{u}_z^{1,0,1,0})\ \hat{u}_r^{0,0,-1,0}\right] - (a_{0,1} - ig_{0,1})\ \hat{u}_z^{1,0,0,0}$$

$$R_{11}^4 = 0$$

Equation system $s = 12$ corresponds to the correction of the Dean fundamental by the TS wave. Its right-hand-side vector is given by

$$R_{12}^1 = -i\aleph(\hat{u}_\theta^{-1,0,0,0}\hat{u}_r^{1,0,1,0} + \hat{u}_\theta^{-1,0,1,0}\hat{u}_r^{1,0,0,0} - \hat{u}_\theta^{1,0,0,0}\hat{u}_r^{-1,0,1,0} + \hat{u}_\theta^{1,0,1,0}\hat{u}_r^{-1,0,0,0})/r$$
$$- i\beta(\hat{u}_r^{-1,0,1,0}\hat{u}_z^{1,0,0,0} + \hat{u}_r^{0,0,1,0}\hat{u}_z^{0,1,0,0} + \hat{u}_r^{1,0,1,0}\hat{u}_z^{-1,0,0,0}) + 2(\hat{u}_\theta^{-1,0,0,0}\hat{u}_\theta^{1,0,1,0} + \hat{u}_\theta^{-1,0,1,0}\hat{u}_\theta^{1,0,0,0}$$
$$+ \hat{u}_\theta^{0,0,1,0}\hat{u}_\theta^{0,1,0,0})/r - \left[\frac{d}{dr}(\hat{u}_r^{-1,0,0,0})\ \hat{u}_r^{1,0,1,0} + \frac{d}{dr}(\hat{u}_r^{-1,0,1,0})\ \hat{u}_r^{1,0,0,0} + \frac{d}{dr}(\hat{u}_r^{0,0,1,0})\ \hat{u}_r^{0,1,0,0}\right.$$
$$\left. + \frac{d}{dr}(\hat{u}_r^{0,1,0,0})\ \hat{u}_r^{0,0,1,0} + \frac{d}{dr}(\hat{u}_r^{1,0,0,0})\ \hat{u}_r^{-1,0,1,0} + \frac{d}{dr}(\hat{u}_r^{1,0,1,0})\ \hat{u}_r^{-1,0,0,0}\right] - (b_{1,0} - ih_{1,0})\ \hat{u}_r^{0,0,1,0}$$

$$R_{12}^2 = -i\beta(\hat{u}_\theta^{-1,0,1,0}\hat{u}_z^{1,0,0,0} + \hat{u}_\theta^{0,0,1,0}\hat{u}_z^{0,1,0,0} + \hat{u}_\theta^{1,0,1,0}\hat{u}_z^{-1,0,0,0}) - (\hat{u}_\theta^{-1,0,0,0}\hat{u}_r^{1,0,1,0}$$
$$+ \hat{u}_\theta^{-1,0,1,0}\hat{u}_r^{1,0,0,0} + \hat{u}_\theta^{0,0,1,0}\hat{u}_r^{0,1,0,0} + \hat{u}_\theta^{0,1,0,0}\hat{u}_r^{0,0,1,0} + \hat{u}_\theta^{1,0,0,0}\hat{u}_r^{-1,0,1,0} + \hat{u}_\theta^{1,0,1,0}\hat{u}_r^{-1,0,0,0})/r$$
$$- \left[\frac{d}{dr}(\hat{u}_\theta^{-1,0,0,0})\ \hat{u}_r^{1,0,1,0} + \frac{d}{dr}(\hat{u}_\theta^{-1,0,1,0})\ \hat{u}_r^{1,0,0,0} + \frac{d}{dr}(\hat{u}_\theta^{0,0,1,0})\ \hat{u}_r^{0,1,0,0} + \frac{d}{dr}(\hat{u}_\theta^{0,1,0,0})\ \hat{u}_r^{0,0,1,0}\right.$$
$$\left. + \frac{d}{dr}(\hat{u}_\theta^{1,0,0,0})\ \hat{u}_r^{-1,0,1,0} + \frac{d}{dr}(\hat{u}_\theta^{1,0,1,0})\ \hat{u}_r^{-1,0,0,0}\right] - (b_{1,0} - ih_{1,0})\ \hat{u}_\theta^{0,0,1,0}$$

$$R_{12}^3 = -i\aleph(\hat{u}_\theta^{-1,0,0,0}\hat{u}_z^{1,0,1,0} + \hat{u}_\theta^{-1,0,1,0}\hat{u}_z^{1,0,0,0} - \hat{u}_\theta^{1,0,0,0}\hat{u}_z^{-1,0,1,0} - \hat{u}_\theta^{1,0,1,0}\hat{u}_z^{-1,0,0,0})/r$$
$$- i\beta(\hat{u}_z^{-1,0,1,0}\hat{u}_z^{1,0,0,0} + \hat{u}_z^{0,0,1,0}\hat{u}_z^{0,1,0,0} + \hat{u}_z^{1,0,1,0}\hat{u}_z^{-1,0,0,0})$$
$$- \left[\frac{d}{dr}(\hat{u}_z^{-1,0,0,0})\ \hat{u}_r^{1,0,1,0} + \frac{d}{dr}(\hat{u}_z^{-1,0,1,0})\ \hat{u}_r^{1,0,0,0} + \frac{d}{dr}(\hat{u}_z^{0,0,1,0})\ \hat{u}_r^{0,1,0,0} + \frac{d}{dr}(\hat{u}_z^{0,1,0,0})\ \hat{u}_r^{0,0,1,0}\right.$$
$$\left. + \frac{d}{dr}(\hat{u}_z^{1,0,0,0})\ \hat{u}_r^{-1,0,1,0} + \frac{d}{dr}\ (\hat{u}_z^{1,0,1,0})\ \hat{u}_r^{-1,0,0,0}\right] - (b_{1,0} - ih_{1,0})\ \hat{u}_z^{0,0,1,0}$$

$$R_{12}^4 = 0$$

7. References

1. Herbert, Th.; and Morkovin, M. V.: Dialogue on Bridging Some Gaps in Stability and Transition Research. *Laminar-Turbulent Transition,* R. Eppler and H. Fasel, eds., Springer-Verlag, 1980, pp. 47–72.
2. Kim, John; and Moser, Robert D.: On the Secondary Instability in Plane Poiseuille Flow. *Phys. Fluids A,* vol. 1, no. 5, May 1989, pp. 775–777.
3. Singer, Bart A.; Reed, Helen L.; and Ferziger, Joel H.: Effects of Streamwise Vortices on Transition in the Plane Channel. *Phys. Fluids A,* vol. 1, no. 12, Dec. 1989, pp. 1960–1971.
4. Nayfeh, Ali H.; and Al-Maaitah, Ayman: Influence on Streamwise Vortices on Tollmien-Schlichting Waves. *Phys. Fluids,* vol. 31, no. 12, Dec. 1988, pp. 3543–3549.
5. Malik, M. R.; and Hussaini, M. Y.: Numerical Simulation of Interactions Between Görtler Vortices and Tollmien-Schlichting Waves. *J. Fluid Mech.,* vol. 210, Jan. 1990, pp. 183–199.
6. Bennett, James; and Hall, Philip: *On the Secondary Instability of Taylor-Görtler Vortices to Tollmien-Schlichting Waves in Fully-Developed Flows.* NASA CR-178221, ICASE Rep. No. 86-73, 1986.
7. Hall, P.; and Smith, F. T.: Nonlinear Interaction of Tollmien-Schlichting Waves and Taylor-Görtler Vortices in Curved Channel Flows. *Proc. Royal Soc. London,* ser. A, vol. 417, no. 1853, June 8, 1988, pp. 255–282.
8. Bassom, Andrew P.; and Hall, Philip: *On the Generation of Mean Flows by the Interaction of Görtler Vortices and Tollmien-Schlichting Waves in Curved Channel Flows.* NASA CR-181690, ICASE Rep. No. 88-43, 1988.
9. Bennett, J.; Hall, P.; and Smith, F. T.: The Strong Nonlinear Interaction of Tollmien-Schlichting Waves and Taylor-Görtler Vortices in Curved Channel Flow. *J. Fluid Mech.,* vol. 223, Feb. 1991, pp. 475–495.
10. Daudpota, Q. Isa; Hall, Philip; and Zang, Thomas A.: On the Nonlinear Interaction of Görtler Vortices and Tollmien-Schlichting Waves in Curved Channel Flows at Finite Reynolds Numbers. *J. Fluid Mech.,* vol. 193, Aug. 1988, pp. 569–595.
11. Stuart, J. T.: On the Non-Linear Mechanics of Wave Disturbances in Stable and Unstable Parallel Flows. Part 1. The Basic Behaviour in Plane Poiseuille Flow. *J. Fluid Mech.,* vol. 9, pt. 3, Nov. 1960, pp. 353–370.
12. Watson, J.: On the Non-Linear Mechanics of Wave Disturbances in Stable and Unstable Parallel Flows. Part 2. The Development of a Solution for Plane Poiseuille Flow and for Plane Couette Flow. *J. Fluid Mech.,* vol. 9, pt. 3, Nov. 1960, pp. 371–389.
13. Singer, Bart A.; and Zang, Thomas A.: *Interactions of Tollmien-Schlichting Waves and Dean Vortices—Comparison of Direct Numerical Simulation and Weakly Nonlinear Theory.* NASA TP-2919, 1989.
14. Herbert, Thorwald: Nonlinear Stability of Parallel Flows by High-Order Amplitude Expansions. *AIAA J.,* vol. 18, no. 3, Mar. 1980, pp. 243–248.
15. Herbert, Thorwald: On Perturbation Methods in Nonlinear Stability Theory. *J. Fluid Mech.,* vol. 126, Jan. 1983, pp. 167–186.
16. Gibson, R. D.; and Cook, A. E.: The Stability of Curved Channel Flow. *Q. J. Mech. & Appl. Math.,* vol. 27, pt. 2, May 1974, pp. 149–160.
17. Drazin, P. G.; and Reid, W. H.: *Hydrodynamic Stability.* Cambridge Univ. Press, c.1981.
18. Mathlab Group: *MACSYMA Reference Manual,* Version Ten, First Printing. Massachusetts Inst. of Technology, Jan. 1983.
19. Davey, A.; and Nguyen, H. P. F.: Finite-Amplitude Stability of Pipe Flow. *J. Fluid Mech.,* vol. 45, pt. 4, Feb. 26, 1971, pp. 701–720.
20. Gottlieb, David; and Orszag, Steven A.: *Numerical Analysis of Spectral Methods: Theory and Applications.* Soc. for Industrial and Applied Mathematics, c.1976.
21. Zang, Thomas A.; and Hussaini, M. Yousuff: On Spectral Multigrid Methods for the Time-Dependent Navier-Stokes Equations. *Appl. Math. & Comput.,* vol. 19, 1986, pp. 359–372.
22. Zang, Thomas A.: On the Rotation and Skew-Symmetric Forms for Incompressible Flow Simulations. *Appl. Numer. Math.,* vol. 6, 1990, pp. 27–40.
23. Krist, Steven E.; and Zang, Thomas A.: *Numerical Simulation of Channel Flow Transition—Resolution Requirements and Structure of the Hairpin Vortex.* NASA TP-2667, 1987.

REPORT DOCUMENTATION PAGE

Form Approved
OMB No. 0704-0188

1. AGENCY USE ONLY *(Leave blank)*	2. REPORT DATE	3. REPORT TYPE AND DATES COVERED
	March 1992	Technical Paper

4. TITLE AND SUBTITLE
A Weakly Nonlinear Theory for Wave-Vortex Interactions in Curved Channel Flow

5. FUNDING NUMBERS
WU 505-59-50-01

6. AUTHOR(S)
Bart A. Singer, Gordon Erlebacher, and Thomas A. Zang

7. PERFORMING ORGANIZATION NAME(S) AND ADDRESS(ES)
NASA Langley Research Center
Hampton, VA 23665-5225

8. PERFORMING ORGANIZATION REPORT NUMBER
L-16989

9. SPONSORING/MONITORING AGENCY NAME(S) AND ADDRESS(ES)
National Aeronautics and Space Administration
Washington, DC 20546-0001

10. SPONSORING/MONITORING AGENCY REPORT NUMBER
NASA TP-3158

11. SUPPLEMENTARY NOTES
Singer: High Technology Corporation, Hampton, VA; Erlebacher: ICASE, Hampton, VA; Zang: Langley Research Center, Hampton, VA.

12a. DISTRIBUTION/AVAILABILITY STATEMENT
Unclassified–Unlimited

Subject Category 02

12b. DISTRIBUTION CODE

13. ABSTRACT *(Maximum 200 words)*

A weakly nonlinear theory is developed to study the interaction of Tollmien-Schlichting (TS) waves and Dean vortices in curved channel flow. The predictions obtained from the theory agree well with results obtained from direct numerical simulations of curved channel flow, especially for low-amplitude disturbances. Some discrepancies in the results of a previous theory with direct numerical simulations are resolved.

14. SUBJECT TERMS
Weakly nonlinear theory; Vortex-wave interaction; Dean vortices; Centrifugal instability; Curved channel flow

15. NUMBER OF PAGES
25

16. PRICE CODE
A03

17. SECURITY CLASSIFICATION OF REPORT	18. SECURITY CLASSIFICATION OF THIS PAGE	19. SECURITY CLASSIFICATION OF ABSTRACT	20. LIMITATION OF ABSTRACT
Unclassified	Unclassified		

NSN 7540-01-280-5500

Standard Form 298(Rev. 2-89)
Prescribed by ANSI Std. Z39-18
298-102